10.1109/ULTSYM.2009.0215

# Unified Model for Bulk Acoustic Wave Resonators' Nonlinear Effects

Eduard Rocas[1,2], Carlos Collado[1], James C. Booth[2], Enrique Iborra[3], Robert Aigner[4]

[1]Universitat Politècnica de Catalunya (UPC), Barcelona, Spain
[2]National Institute of Standards and Technology, Boulder, CO, USA
[3]Grupo de Microsistemas y Materiales Electrónicos, Universidad Politécnica de Madrid, Spain
[4]Triquint Semiconductor, FL, USA

***Abstract* — We present a nonlinear model for Bulk Acoustic Wave resonators that combines different sources of nonlinearity by use of device-independent material-specific parameters to predict intermodulation and harmonic generation. The model accounts for intrinsic nonlinearities due to the stiffened elasticity and thermal effects that arise from temperature changes in a sample driven by an amplitude-modulated signal. Nonlinear parameters of the aluminum nitride piezoelectric layer have been extracted that are in agreement with previously published results.**

***Index Terms* — Intermodulation, thermal effects, second harmonic, Bulk Acoustic Wave resonators.**

## I. Introduction

The demand for accurate modeling of the nonlinearities in bulk acoustic wave (BAW) resonators has recently increased because of the need to fulfill expected requirements in microwave filters [1]. Despite increased demand, accurate modeling is challenging because of the numerous sources of nonlinearity, which may or may not be negligible [2]. Existing models usually make use of nonlinear lumped circuit elements, which are specific to the geometry of the measured device and are difficult to relate to the material properties. Such approaches usually lead to narrow-band, phenomenological descriptions that fail to predict nonlinear effects for different geometries and materials [3], [4].

This work presents a device-independent physical model to account for nonlinear effects in BAW resonators that is valid for a broad range of frequencies. Intrinsic nonlinearities arising from the dependence of the stiffened elasticity on the stress give rise to second harmonics, whereas its variation with the dynamic changes of temperature accounts for the measurable intermodulation distortion.

## II. Unified nonlinear model

The dependence of the elasticity of the piezoelectric layer (generally aluminum nitride (A1N) in BAW devices) on the stress has been shown to be an important contribution to second-harmonic generation [5]. This sets the intrinsic nonlinear properties of the material that can be modeled by using a nonlinear distributed capacitor in a distributed implementation of the acoustic transmission line in the Krimtholz, Leedom and Matthaei (KLM) model [6].

The process by which intermodulation distortion is generated, follows a totally different mechanism. Dissipation, arising mostly from viscous damping, is related to the square of the input signal, which in turn leads to several spectral components of the dissipated power. One of these components is the envelope in "two-balanced tones" test, whose frequency is half the difference $\Delta f$ between two signals $f_1$ and $f_2$. Because a temperature rise follows a low-pass filter-like behavior, or the speed of temperature variations in a material is determined by its diffusivity, the frequency $\Delta f / 2$ of the envelope becomes the dominant spectral component in terms of temperature variations. This leads to a dependence on temperature-dependent material properties at the envelope's frequency. This dependence then gives rise to intermodulation distortion ($2f_1 - f_2$ and $2f_2 - f_1$) when low frequency changes are up-converted by mixing with the fundamental frequencies $f_1$ and $f_2$ [7]. The mechanism of generation for intrinsic and thermal effects is shown in Fig. 1, where the nonlinear capacitor is defined as

$$C_d(S,T) = C_{d,0} + \Delta C_1 S + \Delta C_2 S^2 + \Delta C_T T, \quad (1)$$

which is related with the stiffened elasticity of the material:

$$c^D(S,T) = c_0^D + \Delta c_1^D S + \Delta c_2^D S^2 + \Delta c_T^D T, \quad (2)$$

where S and T are the stress and temperature, respectively, at each infinitesimal section of the piezoelectric layer. The device-independent parameters $\Delta c^D_1$, $\Delta c^D_2$ in (2) account for the intrinsic nonlinearities and can be linked to $\Delta C_1$, $\Delta C_2$ in (1) as shown in [5]. Similarly, the parameter $\Delta c^D_T$ accounts for thermal effects and is linked with $\Delta C_T$ by

$$\Delta C_T = -\frac{1}{c_0^D}\frac{\Delta c_T^D}{A c_0^D}, \quad (3)$$

where $A$ is the area of the device.

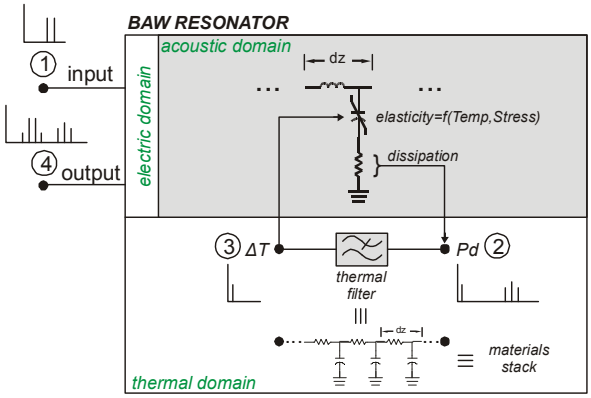


Fig. 1. Nonlinear generation mechanisms in BAW resonators.


*Work partially supported by U.S Government, not subject to U.S. copyright

### A. KLM linear model

The model presented can be considered to be an extension of the KLM model that accounts for nonlinear effects. Specific details of the KLM model implementation can be found in [6]. The piezoelectric layer is implemented as a cascade of infinitesimal cells that enable the circuit parameters to be related to the nonlinear material properties, as shown in Fig. 2. The different material layers of the stack are cascaded as a transmission line in the acoustic domain of the circuit model. Two types of losses are introduced to correctly fit the model to the measured S-parameters. A series resistance models the electric loss due to the electrodes, while a parallel conductance in each cell assesses the acoustic viscous damping of the distributed piezoelectric layer.

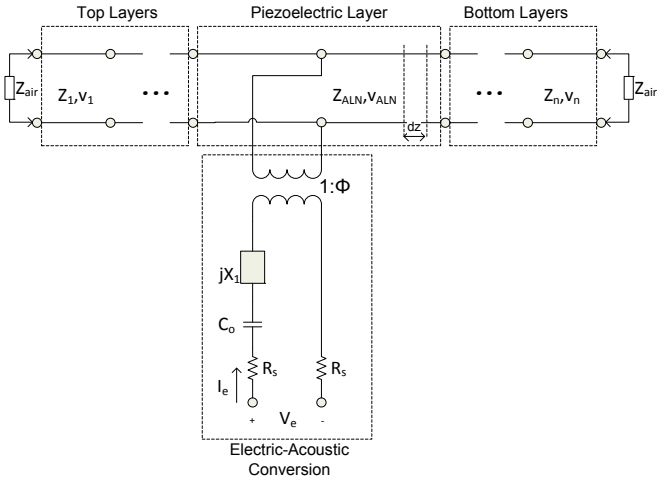


Fig. 2. Nonlinear KLM model: The piezoelectric layer is divided into sections whose lengths are *dz*. The upper and lower layers are modeled cascading acoustic transmission lines.

### B. Nonlinear model implementation

#### i. Intrinsic nonlinearities

As previously stated, the piezoelectric layer is divided into smaller cells and can be directly constructed with the distributed parameters of the equivalent acoustic transmission line. We only discretize the piezoelectric layer, and treat the other layers with equivalent transmission lines, because it is the main source of acoustic losses and it is where most of the acoustic energy is stored. The nonlinear distributed capacitance depends on the mechanical stress at the position of each cell, which accounts for the intrinsic nonlinearities that lead to harmonic and intermodulation generation [5].

#### ii. Heat flow

Besides intrinsic nonlinearities, the dependence on the temperature is also introduced in order to model the thermal effects occurring in the device. This is achieved with a dynamic thermal model of the BAW resonator that is coupled to the acoustic transmission line to model self-heating mechanisms, as seen in Fig. 3. The heat flowing through the layers is modeled, according to the heat equation, as a cascade of series resistances and shunt capacitances that accounts for thermal conductivity and heat capacity, respectively, of each material layer [8]. The terminations of the thermal lines model the silicon substrate at the bottom layer, as well as the convection and radiation resistances at the top layer, which are both followed by a DC voltage source used to model the ambient temperature [9].

#### iii. Self heating mechanisms

As seen in Fig. 4, the dissipated heat due to acoustic viscous damping at each infinitesimal length *dz* of the acoustic line is coupled to the thermal domain as a current source. The sensed temperature, or the voltage in the thermal transmission line, is used to change the elasticity according to (2).

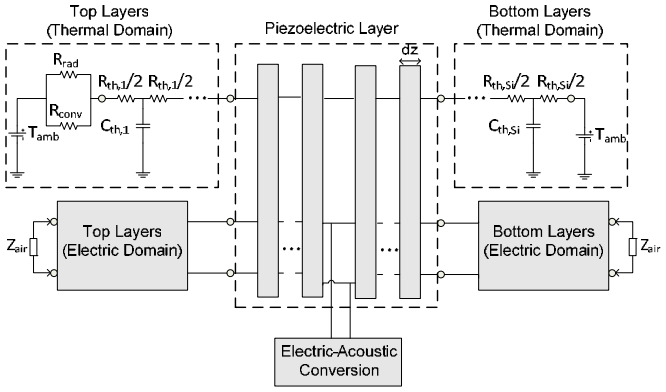


Fig. 3. Nonlinear model including the dynamic thermal domain. Detail of grey blocks is shown in Fig 2 and Fig. 4.

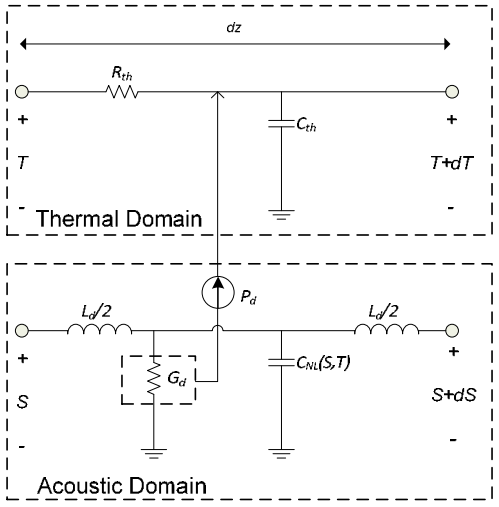


Fig. 4. Implementation of a section *dz* of the piezoelectric layer. The distributed parameters of the acoustic domain are $L_d$, $C_{NL}$ [5]; $G_d$ models the viscosity, and the dissipated power $P_d$ acts as a heat source.

## III. Measurements and Results

Harmonics and intermodulation products of two tones ($f_1$ and $f_2$) have been measured over a broad range of frequencies, 1.88 GHz to 1.98 GHz at 0.01 GHz intervals, in order to obtain the nonlinear parameters $\Delta c^D_1$, $\Delta c^D_2$, and $\Delta c^D_T$ of the piezoelectric layer AlN. Several rectangular and trapezoidal shaped state-of-the-art one-port BAW resonators from two different suppliers, with different stack configurations and areas ranging from 12,500 μm$^2$ to 64,100 μm$^2$, were measured. For clarity we show the measured data of only two of the rectangular-shaped resonators, which correspond to one of the suppliers. The areas of these resonators are 23,300 um$^2$ and 64,100 um$^2$, which will be noted as A23 and A64, respectively.

### *A. Second harmonic and IMD2*

Figures 5 shows measurements and simulations of the second harmonic $2f_1$ and $2f_2$ (2H) and the second order intermodulation products $f_1 + f_2$ (IMD2) for resonators A64 (Fig. 5(a)) and A23 (Fig. 5(b)). In Fig. 5, the central frequency $f_0 = (f_1 + f_2) / 2$ is shown as the horizontal axis, which is linearly swept from 1.88 GHz to 1.98 GHz. The difference between $f_1$ and $f_2$ is kept constant at $\Delta f$ = 220 Hz. The output power of both tones is approximately 19 dBm.

The circles and stars in Fig. 5 show the measured second harmonics $2f_1$ and $2f_2$ (points collapse), and triangles correspond to the measured IMD2. The left vertical axis shows the output power flowing from the device. The right vertical axis shows the output power of the 2H and IMD2 signals normalized with the output power of the fundamental tones after de-embedding the effects of the measurement setup. The ripple in the output power originates from the measurement IMD one-port setup that includes amplifiers, filters, isolators, a combiner and one 90º broadband hybrid. The continuous lines fit the measurements using the unitless $\Delta c^D_1$ = 11 for both resonators. The proposed model and response of both resonators agree very well over the measured frequency range, except around 1.91 GHz, where a small spurious resonance appears. The frequency pattern of the de-embedded normalized power corresponds to the frequency dependence of the stress inside the piezoelectric layer at the fundamental frequencies ($f_1$ and $f_2$), which elucidates stress-dependent parameters that are responsible for these intrinsic nonlinearities.

Measurements performed on all resonators from the other supplier were fitted with a value of $\Delta c^D_1$ = 12, which is comparable to the previous value obtained from A23 and A64 and previous reports [10]. Moreover, these findings support the hypothesis that the stiffened elasticity of AlN is responsible for the 2H and IMD2 generation.

### *B. Third-order intermodulation measurements*

Figures 6 show measurements and simulations (resonators A64: Fig 6(a) and A23: Fig. 6(b)) of the third order intermodulation products $2f_1 - f_2$ and $2f_2 - f_1$ (IMD3). The spacing between tones was also set to $\Delta f$ = 220 Hz. Limitations in the measurement setup, specifically the phase noise of sources, lead to a lower bound on the dynamic range and resulted in a noise floor at approximately -60 dBm. By performing simulations, we were able to show that the IMD3 due to the intrinsic value $\Delta c^D_1$ is smaller than the measured values. In order to account for the measured IMD3, we introduced the additional terms $\Delta c^D_2$ and/or $\Delta c^D_T$.

The data given in Fig.6 have been fitted using $\Delta c^D_1$ = 11, $\Delta c^D_2$ = -1e-10 N$^{-1}$·m$^2$ and $\Delta c^D_T$ = -5.8e6 Pa/K, where the temperature derivative term can also be read as $\Delta c^D_T / c^D_0$ = -15 ppm/K, which agrees in order of magnitude with the values reported in [9] and [11]. We have included $\Delta c^D_2$ to fit the dependence of the intermodulation distortion level on $\Delta f$ / 2, which will be described later. This value of $\Delta c^D_2$ also has the same order of magnitude previously measured by means of mechanical measurements [10].

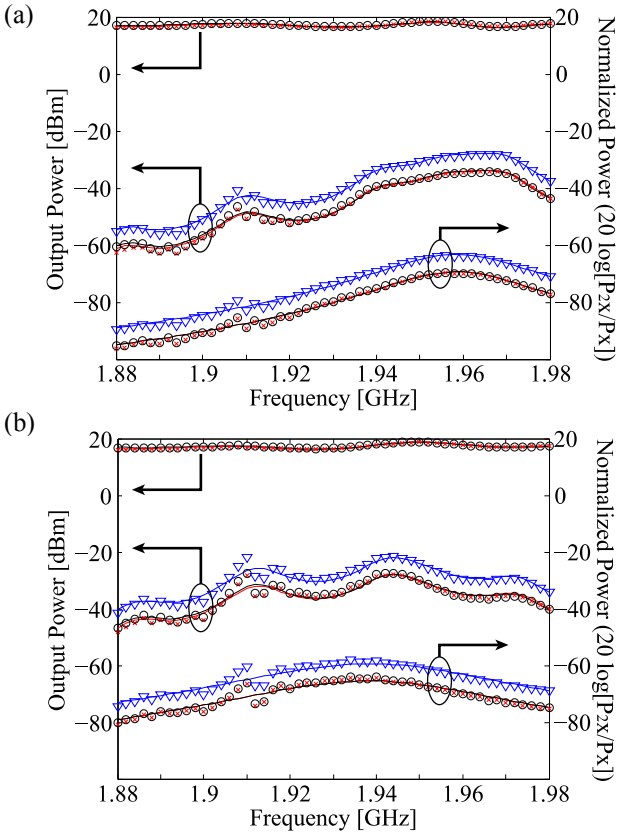


Fig. 5. 2H (circles) and IMD2 (triangles) for A64 (a) and A23 (b) resonators. Left vertical axis indicates the output power and right vertical axis shows normalized values.

For the largest resonator (A64), Fig. 6(a) shows good agreement between the proposed model and the measured IMD3 data, over the measured frequency range above the noise floor. In contrast, the smaller resonator (A23) in Fig. 6(b) shows good agreement at the maximum level of the IMD3, but the model fails to predict the IMD3 when the spurious resonances play an important role. This could be due to the inherent one-dimensional nature of the implemented

model, and further development is underway. In addition, a small bump around 1.97 GHz can be seen in Fig. 6(b), which is also not predicted by our model. We believe that other dissipation sources could play a role in the third-order intermodulation distortion, which may also be dependent on the resonator area.

*i. Third-order intermodulation vs. frequency envelope*

Perhaps, the most indicative measure of the role of thermal effects is the dependence of the intermodulation distortion level on $\Delta f$ [7]. Measurements with the two test tones at the frequency where intermodulation output power is a maximum have been performed as a function of the tone spacing. Figure 7 shows the characteristic low-pass filter shape of the thermal impedance where the horizontal axis represents $\Delta f$. Squares and circles represent the measured IMD3 and solid lines show the simulations using the reported $\Delta c^D_1 = 11$, $\Delta c^D_2 = -1e-10$ $N^{-1}\cdot m^2$, $\Delta c^D_T = -5.8e6$ Pa/K.

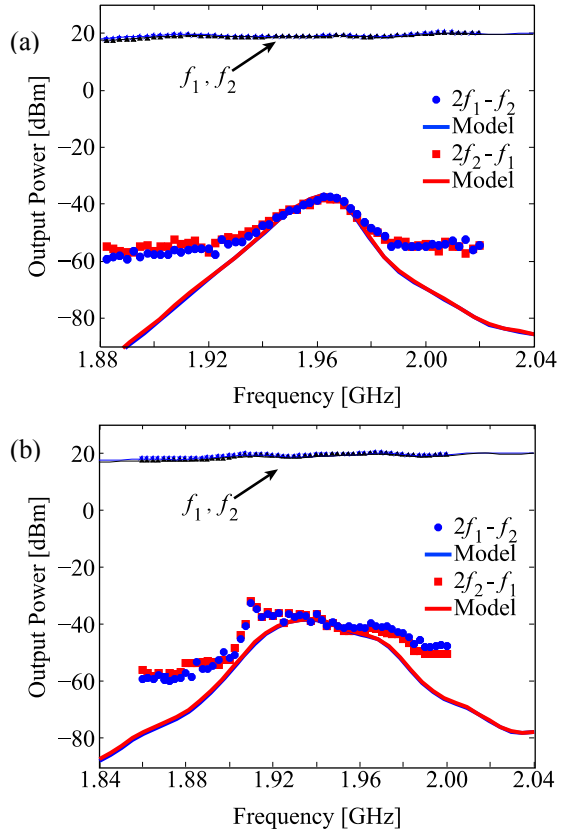


Fig. 6. Stars, triangles, squares and circles represent the measured $f_1$, $f_2$, $2f_1 - f_2$ and $2f_2 - f_1$ for the A64 (a) and A23 (b) resonator. The solid lines are simulations using an input power of 19 dBm.

This shows over this broad parameter space that the third-order intermodulation is due to the contribution of different sources of IMD3: $\Delta c^D_1$, $\Delta c^D_2$ and $\Delta c^D_T$. Figure 7 shows the contribution of each constant, independent of the others. The dashed line with circles shows the IMD3 level generated by $\Delta c^D_1$ as a result of mixing between the second harmonic with the fundamental. The dashed line with triangles shows the IMD3 level generated by the existence of $\Delta c^D_2$, which directly generates third-order components. Intermodulation due to thermal effects is represented by the dashed line with squares. From Fig. 7, IMD3 for slow envelope variations of the driving signal is due, almost entirely, to thermal effects. When the envelope frequency increases, self-heating effects lose importance and intrinsic (thermally independent) values of $\Delta c^D_1$ and $\Delta c^D_2$ become more significant, which produces a smoothing of the IMD3 vs. $\Delta f$ slope.

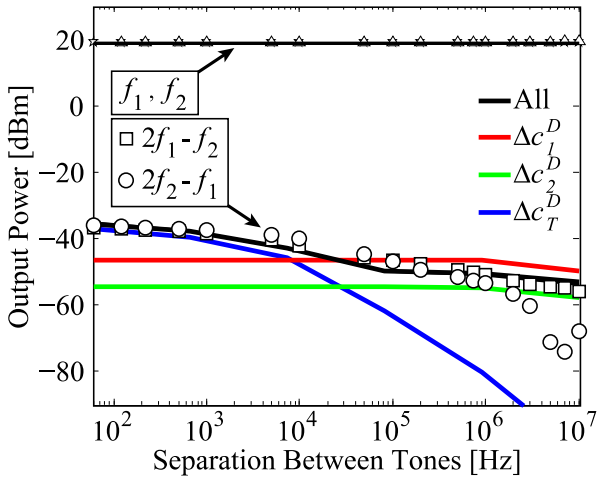


Fig. 7. IMD3 level for different separations between tones for the A64 resonator. Stars, triangles, squares and circles are $f_1$, $f_2$, $2f_1$-$f_2$ and $2f_2$-$f_1$, respectively. Contributions to the IMD3 level of each source by itself are also plotted with dashed lines: circles, triangles and squares represent $\Delta c^D_1$, $\Delta c^D_2$ and $\Delta c^D_T$ contributions, respectively.

A small disagreement between measurements and simulation can be seen in Fig. 7 for values of $\Delta f$ between 10 kHz to 100 kHz. Further improvements of the thermal model may account for this discrepancy by introducing additional terms to account for frequency-dependent heat diffusion. This may produce the desired slower decay and improve the agreement between the model and measurements. Furthermore, such developments may reproduce the measured asymmetries of $2f_1 - f_2$ and $2f_2 - f_1$ from 1 MHz up to 10 MHz.

## VII. Summary and Conclusions

We have presented a nonlinear BAW model that allows us to obtain geometry-independent material parameters that account for second-harmonic and intermodulation generation with bulk material properties. The model is able to predict the harmonic generation and second-order intermodulation due to the stiffened elasticity as a function of stress. We have obtained a value of $\Delta c^D_1 = 11$ for the samples provided by one manufacturer (rectangular-shaped with several different areas), and $\Delta c^D_1 = 12$ for a set of samples from another manufacturer (trapezoidal-shaped with several different areas). These results show that the nonlinear-stiffened elasticity is predominantly responsible for second-harmonic generation at

these broad measurement frequencies and array of devices areas and shapes.

Thermal effects were also modeled from third-order intermodulation measurements, and a value of $\Delta c^{D}_{T}$ = -5.8e6 Pa/K was obtained for all the square-shaped resonators. This value is consistent with the value reported in [9] and [11]. Further research should accurately model heat diffusion through the material's stack. Additional investigation is underway to assess the role of other heat sources, such as the electrical resistance of the electrodes, effects of nonlinear permittivity, etc.

## ACKNOWLEDGMENT

This work was partially supported by the Spanish Government (CICYT) under Grant TEC-2006-13248-C04-02/TCM. E.R. thanks the support from BES-2007-16775. The authors thank A. Padilla, N. D. Orloff, J. Mateu and J. O'Callaghan for their fruitful discussions and critical review of this manuscript.

## REFERENCES

[1] C.W. Liu and M. Damgaard. "IP2 and IP3 Nonlinearity Specifications for 3G/WCDMA Receivers". *Microwave Journal*, May 2009.

[2] D.A. Hall, "Nonlinearity in Piezoelectric Ceramics", *J. Mat. Sci.* 36, pp. 4575-4601, 2001.

[3] M. Ueda, M. Iwaki, T Nishihara, Y. Satoh, K. Hashimoto, "A Circuit Model for Nonlinear Simulation of Radio-Frequency Filters Using Bulk Acoustic Wave Resonators," *IEEE Trans. Ultrason. Ferroelec. Freq. Control*, , vol. 55, no. 4, pp. 849-856, April 2008.

[4] E. Rocas, C. Collado, J. Mateu, H. Campanella and J.M O'Callaghan, "Third order Intermodulation Distortion in Film Bulk Acoustic Resonators at Resonance and Antiresonance". *IEEE MTT-S International Microwave Symposium Digest*, pp. 1259-1262, June 2008.

[5] C. Collado, E. Rocas, J. Mateu, A. Padilla, J. M. O'Callaghan," Nonlinear Distributed Model for BAW Resonators", *IEEE Trans. on Microwave Theory and Techniques*. Accepted for publication, 2009.

[6] R. Krimholtz, D.A. Leedom and G.L. Matthaei, "New equivalent circuits for elementary piezoelectric transducers," *Electronics Letters* , vol. 6, no. 13, pp. 398-399, June 1970.

[7] J. Vuolevi, T. Rahkonen and J.P.A. Manninen, "Measurement technique for characterizing memory effects in RF power amplifiers," *IEEE Trans. on Microwave Theory and Techniques*, vol. 49, no. 8, pp. 1383-1389, 2001.

[8] F.P. Incropera and D.P. de Witt, "Fundamentals of Heat and Mass Transfer", 5th ed., J. Wiley & Sons N.Y., 2002.

[9] J.D. Larson and Y. III Oshrnyansky , "Measurement of Effective $k_t^2$, Q, $R_p$, $R_s$, vs. Temperature for Mo/AlN FBAR Resonators," *Proc. 2002 IEEE Ultrasonics Symposium*, pp. 939-943, 2002.

[10] S.P. Łepkowski and G. Jurczak, "Nonlinear elasticity in III-N compounds: Ab initio calculations", *Physical Review B,* vol. 72, 245201, pp. 1-12. 2005.

[11] D.K. Pandey, R.R. Yadav, "Temperature dependent ultrasonic properties of aluminium nitride", *Applied Acoustics*, vol. 70, no. 3, pp. 412-415, March 2009.